

Supporting Information for

Pressure-driven Configurational Crossover between $4f^7$ and $4f^65d^1$ States – Giant Enhancement of Narrow Eu^{2+} UV-Emission Lines in SrB_4O_7 for Luminescence Manometry

Teng Zheng,¹ Marcin Runowski,^{1,*} Plácida Rodríguez-Hernández,² Alfonso Muñoz,² Francisco J. Manjón,³ Małgorzata Sójka,⁴ Markus Suta,⁵ Eugeniusz Zych,⁴ Stefan Lis¹ and Víctor Lavín⁶

¹ Adam Mickiewicz University, Faculty of Chemistry, Uniwersytetu Poznańskiego 8, 61-614 Poznań, Poland

² Departamento de Física, MALTA Consolider Team, Instituto de Materiales y Nanotecnología, Universidad de La Laguna, Apartado de Correos 456, E-38200 San Cristóbal de La Laguna, Santa Cruz de Tenerife, Spain

³ Instituto de Diseño para la Fabricación y Producción Automatizada, MALTA Consolider Team, Universitat Politècnica de València, Cno. de Vera s/n, 46022 València, Spain

⁴ Faculty of Chemistry, University of Wrocław, F. Joliot-Curie 14, 50-383 Wrocław

⁵ Inorganic Photoactive Materials, Institute of Inorganic Chemistry, Heinrich Heine University Düsseldorf, Universitätsstr. 1, D-40225 Düsseldorf, Germany

⁶ Departamento de Física, MALTA Consolider Team, and IUDEA, Universidad de La Laguna, Apartado de Correos 456, E-38200 San Cristóbal de La Laguna, Santa Cruz de Tenerife, Spain

Table of Contents

I. Properties at ambient conditions

- i. Figure S1. The emission spectra of the samples.
- ii. Figure S2. The SEM images and XRD pattern of the sample.
- iii. Figure S3. The theoretical total one-phonon density of states in black and partial atomic contributions to the one-phonon density of states.
- iv. Figure S4. The magnified vibronic sidebands.

II. Photoluminescence properties at low temperature

- i. Figure S5. temperature independence of the redshift of 4f-4f emission

III. Vibrational and Photoluminescence properties at high pressure

- i. Figure S6. Pressure dependent Raman spectra and experimental Raman-active mode frequencies
- ii. Figure S7. Theoretical (lines) and experimental (symbols) Raman-active mode frequencies.
- iii. Figure S8. Non-normalized UV emission spectra of the SrB₄O₇: 0.03Eu²⁺ / 0.01Sm²⁺material at decompression process
- iv. Figure S9. The spectral position (peak centroid) of 4f⁶5d→⁸S_{7/2} (5d → 4f) transition

IV. Tables

- i. Table S1. Cell parameters, atomic coordinates at Pressure = 0 GPa and 61 GPa
- ii. Table S2. Theoretical elastic constants (in GPa) in SrB₄O₇ at room pressure
- iii. Table S3. B, G and E (in 0 GPa) and v given in the Voigt, Reuss and Hill approximations
- iv. Table S4. Theoretical and experimental Raman-active modes in SrB₄O₇ (in 0 GPa)
- v. Table S5. Theoretical Raman-active zero-pressure mode frequencies and pressure coefficients of SrB₄O₇.
- vi. Table S6. Comparison of Red-shift of the 5d→4f broad band in materials.
- vii. Table S7. Comparison of the performances of the reported optical pressure sensors.

I. Properties at ambient conditions

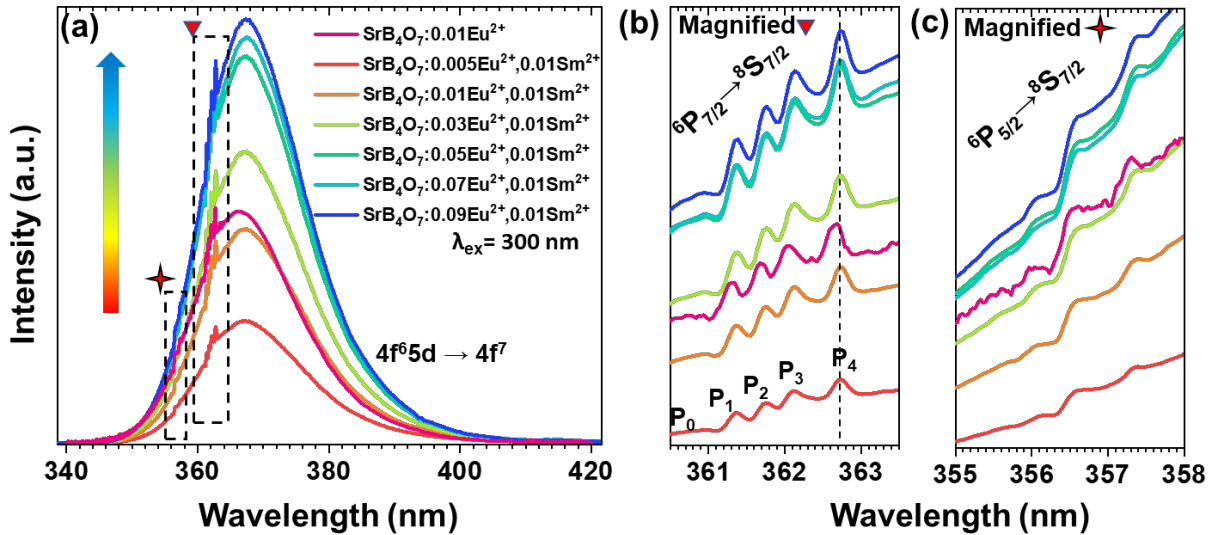


Figure S1. (a) Emission spectra in the UV range (340 - 420 nm), of the synthesized SrB₄O₇:0.01Eu²⁺ (without Sm²⁺) and SrB₄O₇:0.01Sm²⁺, x Eu²⁺ ($x = 0.005 - 0.09$) samples at room temperature and ambient pressure. (b) Magnified spectra in the “triangle” marked area, showing the $6P_{7/2} \rightarrow 8S_{7/2}$ transitions. (c) Magnified spectra in the “star” marked area, showing the $6P_{5/2} \rightarrow 8S_{7/2}$ transitions.

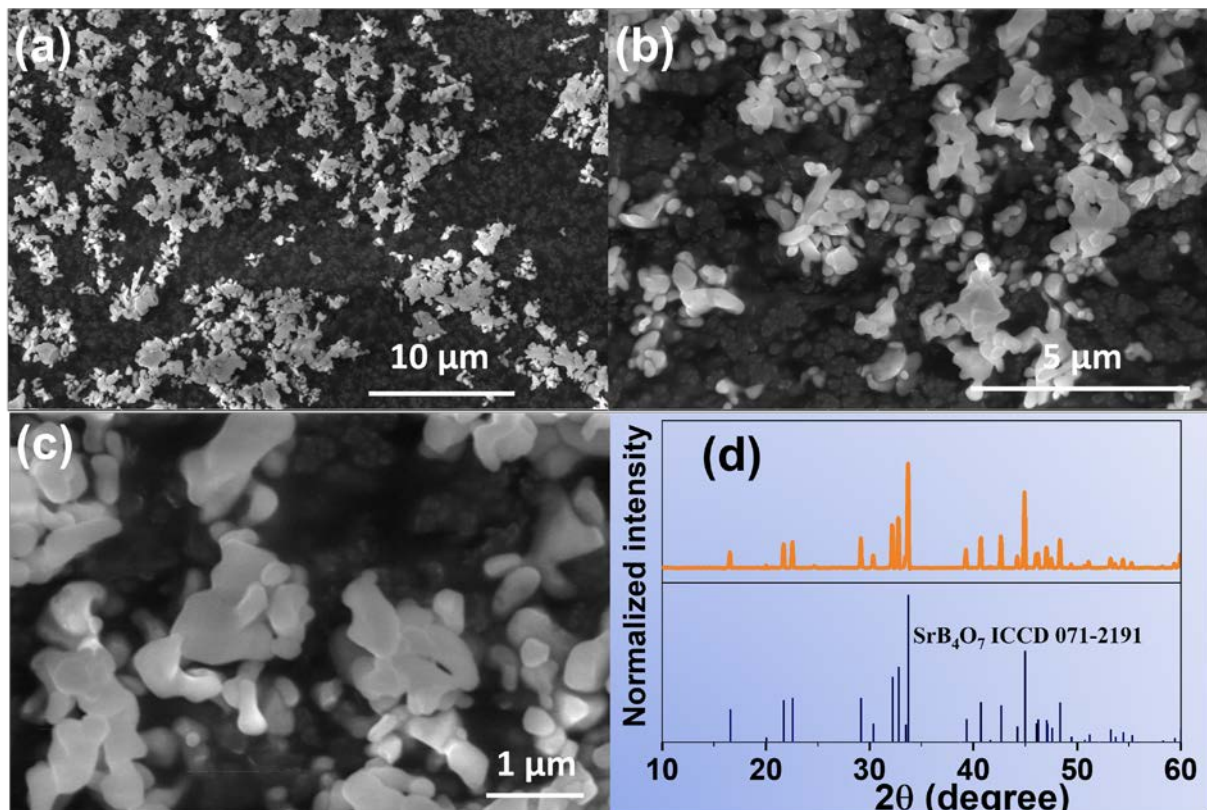


Figure S2. (a-c) SEM images of the optimal luminescent sample, i.e., $\text{SrB}_4\text{O}_7:0.01\text{Sm}^{2+}, 0.03 \text{Eu}^{2+}$ phosphors at three different scales. (d) The indexed experimental XRD pattern of the selected sample. The line patterns correspond to the references from the ICDD standards database.

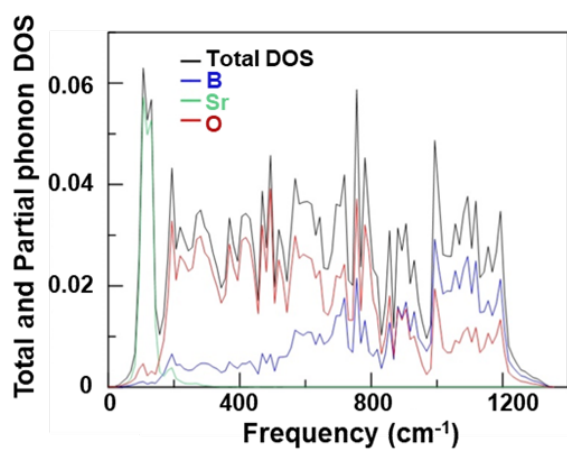


Figure S3. The theoretical total one-phonon density of states in black and the partial atomic contributions of Sr (green), O (red), and B (blue) to the one-phonon density of states in SrB_4O_7 .

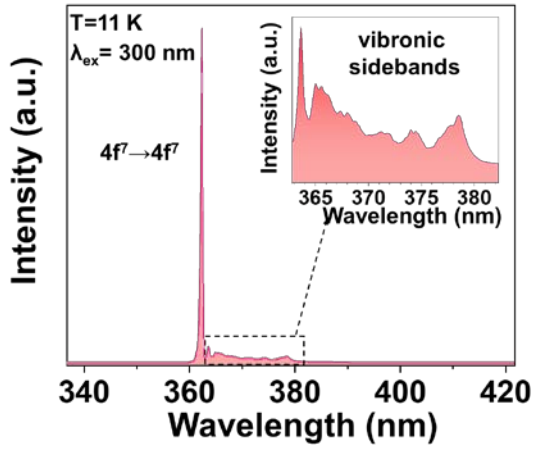


Figure S4. The magnified vibronic sidebands of the emission spectra of the $\text{SrB}_4\text{O}_7:0.01\text{Sm}^{2+}, 0.03\text{Eu}^{2+}$ sample, measured at 11 K and ambient pressure.

II. Photoluminescence properties at low temperature

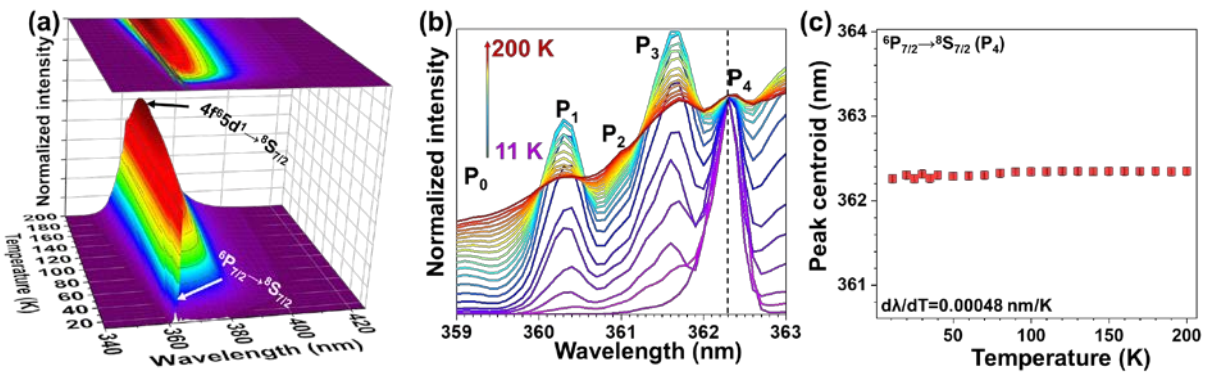


Figure S5. (a) Normalized emission spectra of $\text{SrB}_4\text{O}_7:0.03\text{Eu}^{2+}, 0.01\text{Sm}^{2+}$ at selected measured temperatures and ambient pressure under 300 nm excitation. (b) The magnified normalized spectra, emphasizing on the $4f^7 - 4f^7$ transitions of the Eu^{2+} emission in the sample. (c) Temperature dependence of the peak centroid of P_4 components of the ${}^6\text{P}_{7/2} \rightarrow {}^8\text{S}_{7/2}$ transition of Eu^{2+} .

III. Vibrational and Photoluminescence properties at high pressure

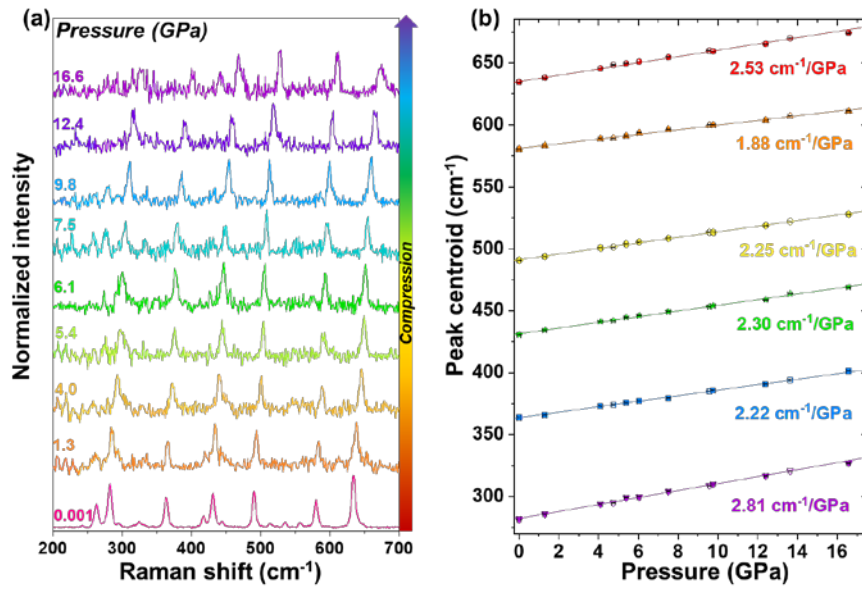


Figure S6. (a) Raman spectra of SrB_4O_7 : 0.03 Eu^{2+} , 0.01 Sm^{2+} at selected pressure values . (b) Pressure dependence of the experimental Raman-active mode frequencies in compression (filled symbols) and decompression (empty symbols); the continuous lines represent the applied linear fits.

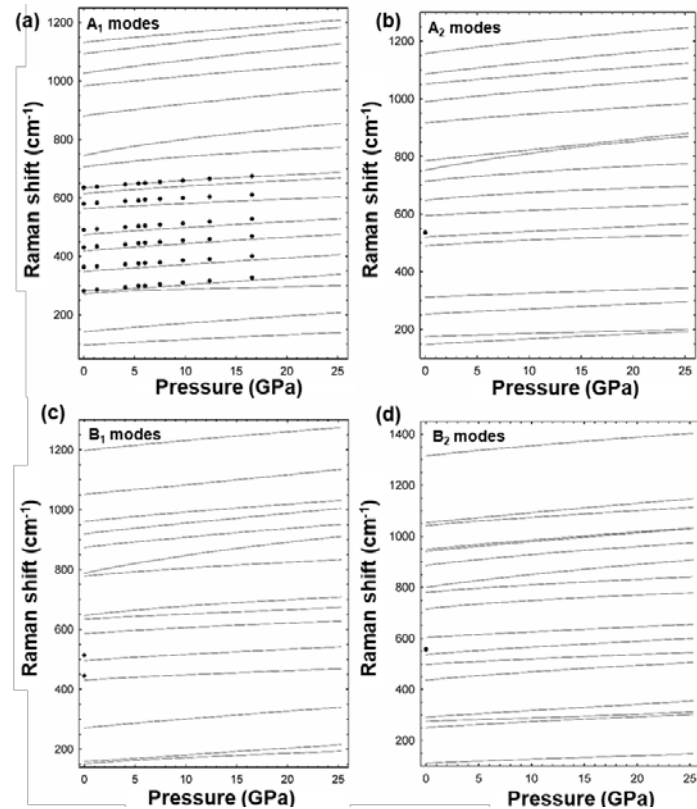


Figure S7. Theoretical (lines) and experimental (symbols) Raman-active mode frequencies of bulk SrB_4O_7 as a function of pressure.

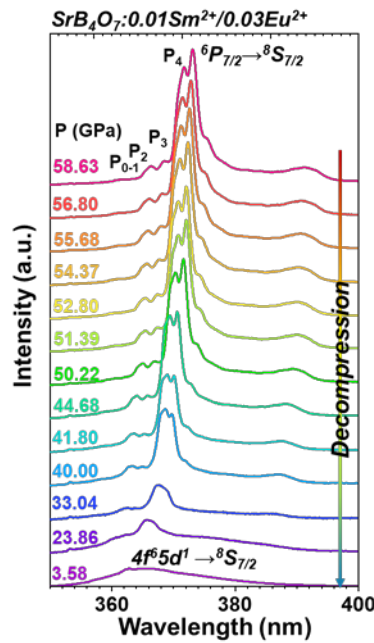


Figure S8. Non-normalized UV emission spectra of SrB_4O_7 : 0.03 Eu^{2+} , 0.01 Sm^{2+} , measured at the decompression cycle and room temperature under 280 nm excitation.

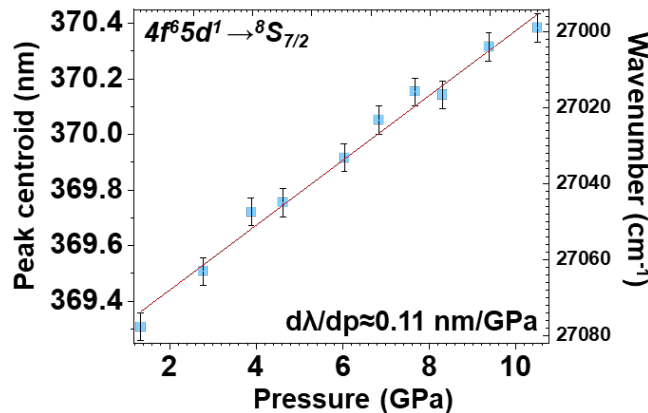


Figure S9. The spectral positions (peak centroid) of the $4\text{f}^65\text{d}^1 \rightarrow 4\text{f}^7(8\text{S}_{7/2})$ transition of Eu^{2+} in the SrB_4O_7 : 0.09 Eu^{2+} , 0.01 Sm^{2+} sample, determined up to around 10.5 GPa, at which the Eu^{2+} -related $4\text{f}^65\text{d}^1 \rightarrow 4\text{f}^7$ emission is well-observed.

IV. Tables

Table S1. Cell parameters (a , b , c), atomic coordinates (x , y , z) at pressure = 0 GPa and 61 GPa based on theoretical calculation, bulk modulus (B_0) and its pressure derivative (B_0') of the SrB_4O_7 (space group $Pmn2_1$, no. 31).

SrB_4O_7 (0 GPa)	SrB_4O_7 (61 GPa)
----------------------------------	-----------------------------------

<i>a</i> (Å)		10.7354		9.78803			
<i>b</i> (Å)		4.42930		4.11315			
<i>c</i> (Å)		4.23761		3.92452			
<i>V</i> (Å ³)		201.500		158.000			
Atomic species	Wyckoff positions	<i>x</i>	<i>y</i>	<i>z</i>	<i>x</i>	<i>y</i>	<i>z</i>
Sr(1)	2a	0	0.78832	0.49833	0	0.80675	0.45212
O(1)	2a	0	0.22619	-0.08078	0	0.18259	-0.08400
O(2)	4b	0.64085	0.35629	0.45492	0.62968	0.34336	0.42879
O(3)	4b	0.63502	0.72709	0.86377	0.63021	0.69282	0.88502
O(4)	4b	0.77752	0.13263	0.85989	0.76271	0.15059	0.88189
B(1)	4b	0.87849	0.32558	0.02622	0.87940	0.32986	0.02492
B(2)	4b	0.74904	0.82231	0.00294	0.78054	0.81736	0.01182
<i>B</i> ₀ (GPa) at 26 GPa		150.165					
<i>B</i> _{0'} at 26 GPa		4.12726					

Table S2. Theoretical elastic constants (in GPa) in SrB₄O₇ at ambient pressure. The experimental values taken from ref. [1] and the calculated values from ref. [2] have been also included for comparison.

	This work	Ref. [1]	Ref. [2]
<i>C</i> ₁₁	282.2	304 (4)	318
<i>C</i> ₁₂	77.9	70 (35)	132
<i>C</i> ₁₃	60.8	49 (29)	90
<i>C</i> ₂₂	328.7	268 (1)	370
<i>C</i> ₂₃	49.4	55 (33)	114
<i>C</i> ₃₃	359.5	378 (3)	355
<i>C</i> ₄₄	110.8	139 (2)	106
<i>C</i> ₅₅	127.8	120 (4)	87
<i>C</i> ₆₆	120.8	133 (2)	124

Table S3. Elastic moduli B , G and E (in 0 GPa), Poisson's ratio (ν) given in the Voigt, Reuss and Hill approximations, labeled with subscripts V, R and H in SrB_4O_7 at ambient conditions. A_U denotes the elastic anisotropy index.

SrB ₄ O ₇ at 0 GPa	
B_V, B_R, B_H	149.62; 149.03; 149.33.
E_V, E_R, E_H	291.54; 288.29; 289.91.
G_V, G_R, G_H	124.03; 122.40; 123.22
ν_V, ν_R, ν_H	0.175; 0.178; 0.176
$B_V/G_V, B_R/G_R, B_H/G_H$	1.206; 1.218; 1.212
A_U	0.071

Table S4. Theoretical and experimental Raman-active modes in SrB_4O_7 (in black) at ambient pressure. Values reported in ref. [3] (underlined) and ref. [4] (in brackets), which are compatible with our theoretical calculations, are also reported. The pressure dependence of the modes in bold font is shown in Figure 5e and S4. All values are in cm^{-1} .

Sym.	The.	Exp.	Sym.	The.	Exp.	Sym.	The.	Exp.
A_1^1	95.4	<u>104</u> , (102)	A_2^7	520.5	<u>536</u> , <u>535</u>	A_2^{13}	916.7	<u>926</u>
B_2^1	110.1	<u>117</u>	B_2^8	536.8	<u>557</u> , <u>555</u> , (535)	B_1^{12}	919.3	<u>928</u> , <u>930</u>
B_2^2	130.1	<u>142</u>	A_1^8	563.0	580 , <u>580</u>	B_2^{14}	940.8	<u>948</u> , <u>938</u>
A_1^2	141.4	<u>151</u> , (150)	B_1^6	585.9	<u>609</u> , (581)	B_2^{15}	948.2	<u>962</u>
A_2^1	147.3	<u>156</u> , (153)	A_2^8	594.6	<u>616</u>	B_1^{13}	960.4	<u>969</u>
B_1^1	150.6	<u>160</u>	B_2^9	602.9	<u>634</u> , (633)	A_1^{15}	982.7	<u>995</u> , <u>989</u> , (988)
B_1^2	159.4		A_1^9	614.3	635 , <u>634</u> , (633)	A_2^{14}	989.9	<u>997</u>
A_2^2	174.3	(192)	A_1^{10}	632.9	<u>641</u>	B_1^{14}	1010.6	<u>1012</u>
B_2^3	250.9	242, (263)	B_1^7	634.2	<u>650</u> , (635)	A_1^{16}	1026.1	<u>1046</u> , <u>1042</u>
A_2^3	251.9	263, <u>263</u> , (262)	B_1^8	646.4		B_2^{16}	1041.2	<u>1055</u>
B_1^3	271.2	<u>282</u> , (280)	A_2^9	647.4		B_1^{15}	1050.9	<u>1068</u>
A_1^3	271.4	283 , <u>282</u>	A_1^{11}	705.7	<u>706</u> , <u>705</u> , (703)	A_2^{15}	1051.0	
B_2^4	275.3	(281)	A_2^{10}	713.2	<u>720</u>	B_2^{17}	1053.5	

A_1^4	282.3	<u>294</u> , (292)	B_2^{10}	715.1	<u>730</u> , (726)	A_2^{16}	1085.0	<u>1138</u>
B_2^5	292.4	<u>301</u>	A_1^{12}	745.2	<u>741</u> , (750)	A_1^{17}	1092.5	1100
A_2^4	311.8	<u>325</u> , <u>324</u> , (325)	A_2^{11}	751.6	<u>753</u>	A_1^{18}	1131.2	<u>1148</u>
A_1^5	348.4	364, <u>362</u>, (361)	B_1^9	777.5	<u>781</u>			<u>1167</u>
A_2^5	402.5	417	B_2^{11}	780.8		A_2^{17}	1156.0	1169, <u>1167</u>
A_1^6	418.5	431, <u>431</u>, (430)	A_2^{12}	784.8	<u>799</u>			1176
B_1^4	430.4	<u>445</u> , <u>444</u> , (442)	B_1^{10}	787.9		B_1^{16}	1196.9	
B_2^6	435.9	<u>449</u> , (439)	A_1^{13}	789.8	<u>809</u> , <u>807</u> , (815)			1285
A_1^7	473.8	491, <u>491</u>, (490)	B_2^{12}	799.6	<u>814</u> , (818)	B_2^{18}	1315.1	1345
A_2^6	489.6	<u>500</u> , (490)	B_1^{11}	874.1	<u>890</u>			1374
B_1^5	495.5	<u>514</u> , <u>513</u> , (514)	A_1^{14}	879.7	<u>888</u> , <u>885</u> , (886)			1501
B_2^7	498.8	<u>517</u> , (491)	B_2^{13}	886.1	<u>893</u>			1659

Table S5. Theoretical Raman-active zero-pressure mode frequencies and pressure coefficients of SrB_4O_7 according to a linear fit up to 5 GPa.

Sym.	(cm ⁻¹)	dω/dP (cm ⁻¹ /GPa)	Sym.	(cm ⁻¹)	dω/dP (cm ⁻¹ /GPa)	Sym.	(cm ⁻¹)	dω/dP (cm ⁻¹ /GPa)
A_1^1	95.4	2.2	A_2^7	520.5	2.0	A_2^{13}	916.7	3.1
B_2^1	110.1	1.8	B_2^8	536.8	3.2	B_1^{12}	919.3	3.8
B_2^2	130.1	3.4	A_1^8	563.0	2.0	B_2^{14}	940.8	4.1
A_1^2	141.4	3.2	B_1^6	585.9	2.2	B_2^{15}	948.2	4.0
A_2^1	147.3	2.1	A_2^8	594.6	1.9	B_1^{13}	960.4	3.4
B_1^1	150.6	2.5	B_2^9	602.9	2.5	A_1^{15}	982.7	3.6
B_1^2	159.4	2.0	A_1^9	614.3	2.8	A_2^{14}	989.9	3.8
A_2^2	174.3	1.2	A_1^{10}	632.9	3.0	B_1^{14}	1010.6	5.7
B_2^3	250.9	2.4	B_1^7	634.2	1.9	A_1^{16}	1026.1	4.9
A_2^3	251.9	2.0	B_1^8	646.4	3.6	B_2^{16}	1041.2	3.8
B_1^3	271.2	3.2	A_2^9	647.4	3.2	B_1^{15}	1050.9	3.3

A ₁ ³	271.4	2.3	A ₁ ¹¹	705.7	4.0	A ₂ ¹⁵	1051.0	3.4
B ₂ ⁴	275.3	1.4	A ₂ ¹⁰	713.2	3.6	B ₂ ¹⁷	1053.5	3.9
A ₁ ⁴	282.3	1.6	B ₂ ¹⁰	715.1	3.9	A ₂ ¹⁶	1085.0	4.4
B ₂ ⁵	292.4	2.5	A ₁ ¹²	745.2	6.3	A ₁ ¹⁷	1092.5	4.4
A ₂ ⁴	311.8	1.4	A ₂ ¹¹	751.6	6.5	A ₁ ¹⁸	1131.2	3.6
A ₁ ⁵	348.4	2.4	B ₁ ⁹	777.5	3.1	A ₂ ¹⁷	1156.0	4.7
A ₂ ⁵	402.5	1.7	B ₂ ¹¹	780.8	3.2	B ₁ ¹⁶	1196.9	3.7
A ₁ ⁶	418.5	2.7	A ₂ ¹²	784.8	3.9	B ₂ ¹⁸	1315.1	4.3
B ₁ ⁴	430.4	2.0	B ₁ ¹⁰	787.9	6.5			
B ₂ ⁶	435.9	3.6	A ₁ ¹³	789.8	3.5			
A ₁ ⁷	473.8	2.7	B ₂ ¹²	799.6	5.5			
A ₂ ⁶	489.6	2.3	B ₁ ¹¹	874.1	3.6			
B ₁ ⁵	495.5	2.3	A ₁ ¹⁴	879.7	4.5			
B ₂ ⁷	498.8	2.2	B ₂ ¹³	886.1	4.6			

Table. S6. Red-shift of the $4f^65d^1 \rightarrow 4f^7$ broad band in materials reported in literature.

Host matrix	Energy (cm ⁻¹)	Energy shift (cm ⁻¹ /GPa)	Pressure range (GPa)	Reference
BaCN ₂		-384	0 - 5	[5]
SrAl ₂ O ₄	18500	-375	0 - 4	[6]
CaAl ₂ O ₄	22900	-290	0 - 10	[6]
BaBr ₂	24700	-225	0 - 10	[7]
BaBr ₂	21200	-200	10 - 27	[7]
EuF ₂	30300	-175	0 - 8	[8]
SrF ₂		-174	0 - 5	[9]
CaBPO ₅	24800	-150	0 - 10	[6]
BaF ₂		-139	2 - 7	[9]
Ba ₂ SiO ₄	19600	-127	0 - 10	[6]
Ca ₂ P ₂ O ₇	23300	-70	0 - 10	[6]

SrB ₄ O ₇		-8.5	0 - 10	this work
---------------------------------	--	------	--------	-----------

Table S7. Performance of the reported optical pressure sensors based on the materials doped with Ln^{2+/3+} or Cr³⁺, operating with different manometric parameters - MP (line shift, FWHM, band ratio, lifetime). Some of the d(MP)/dP (cm⁻¹/GPa) values are estimated from spectra in the literature.

Active ion	Host	Transition	MP	d(MP)/dP (nm/GPa)	d(MP)/dP (cm ⁻¹ /GPa)	FWHM (nm)	T-shift (nm/K)	λ (nm)	Ref.
Eu ²⁺	SrB ₄ O ₇	⁶ P _{7/2} → ⁸ S _{7/2}	line shift	0.17	-12.84	~0.22	4.8×10 ⁻⁴	362.7	this work
Sm ²⁺	SrB ₄ O ₇	⁵ D ₀ → ⁷ F ₀	line shift	0.255	-5.41	0.2	-1×10 ⁻⁴	685	[10]
Sm ²⁺	SrB ₂ O ₄	⁵ D ₀ → ⁷ F ₀	line shift	0.24	-5.11	0.15	-1 × 10 ⁻⁴	685	[11]
Sm ²⁺	SrFCl	⁵ D ₀ → ⁷ F ₀	line shift	1.1	~-22.8	0.15	-2.3 × 10 ⁻³	690	[12]
Cr ³⁺	Al ₂ O ₃	² E→ ⁴ A ₂	line shift	0.365	~-7.6	0.75	6.8×10 ⁻³	694	[13]
Cr ³⁺	YAlO ₃	² E→ ⁴ A ₂	line shift	0.70	~-13.4	~11.5	7.6 × 10 ⁻³	723	[14]
Er ³⁺	YF ₃	⁴ F _{9/2} → ⁴ I _{15/2} (Stark)	line shift	0.186	-4.18	-	-3×10 ⁻⁴	665	[15]
Er ³⁺	NaBiF ₄	⁴ I _{13/2} → ⁴ I _{15/2} (Stark)	line shift	-0.80	3.54	62	-	1503	[16]
Er ³⁺	SrF ₂	⁴ F _{9/2} → ⁴ I _{15/2}	lifetime	7.7%	-	-	-	653	[17]
		⁴ S _{3/2} → ⁴ I _{15/2}	lifetime	6.4%	-	-	-	538	
		² H _{11/2} → ⁴ I _{15/2}	lifetime	6.2%	-	-	-	516	
Nd ³⁺	YAlO ₃	⁴ F _{3/2} → ⁴ I _{9/2} (Stark)	line shift	-0.13	3.15	-	1 × 10 ⁻⁶	875	[14]
Eu ³⁺	Y ₃ Al ₅ O ₁₂	⁵ D ₀ → ⁷ F ₁	line shift	0.197	-5.7	~0.5	-5.4 × 10 ⁻⁴	591	[16]
Eu ²⁺	BaLi ₂ Al ₂ Si ₂ N ₆	4f ⁶ 5d-4f ⁷	line shift	1.58	~-53.32	~ 60.5	-	532	[18]
Sm ³⁺	Y ₃ Al ₅ O ₁₂	⁴ G _{5/2} → ⁶ H _{7/2} (Stark)	line shift	0.30	~-7.85	~3.81	2.3 × 10 ⁻⁴	618	[19]
Tm ³⁺	LaPO ₄	¹ G ₄ → ³ H ₆	line shift	0.1	~-4.43	14	-2 × 10 ⁻³	475	[20]
		³ H ₄ → ³ H ₆ / ¹ G ₄ → ³ H ₆	band ratio	8%	-	-	-		
Ce ³⁺	Y ₆ Ba ₄ (Si O ₄) ₆ F ₂	² F _J → ² D _J (excitation)	line width	2.5%	-	43	-	342	[21]

		$^2D_J \rightarrow ^2F_J$ (emission)	line width	1.5%	-	124	-	466	
			line shift	0.63	-28.62	124	-	466	

References in Supporting information:

- [1] I. Martynyuk-Lototska, T. Dudok, O. Mys, R. Vlokh, Elastic, piezooptic and acoustooptic properties of SrB₄O₇ and PbB₄O₇ crystals, Opt. Mater. (Amst). 31 (2009) 660–667. <https://doi.org/10.1016/j.optmat.2008.06.020>.
- [2] V.I. Zinenko, M.S. Pavlovskii, A.I. Zaitzev, A.S. Krylov, A.S. Shinkorenko, Vibrational spectra and elastic piezoelectric and polarization properties of the α -SrB₄O₇ crystal, J. Exp. Theor. Phys. 115 (2012) 455–461. <https://doi.org/10.1134/S1063776112080195>.
- [3] A.A. Sobol, V.E. Shukshin, A.I. Zaitsev, Raman spectroscopy of SrB₄O₇ single crystals in the temperature range 300–1273 K, Opt. Spectrosc. 121 (2016) 25–31. <https://doi.org/10.1134/S0030400X16070201>.
- [4] J. Hanuza, M.Mączka, J. Lorenc, A.A. Kaminskii, P. Becker, L. Bohatý, Recent Advances in linear and nonlinear Raman spectroscopy I, J. Raman Spectrosc. 38 (2007) 1538–1553. <https://doi.org/10.1002/jrs>.
- [5] Y. Masubuchi, S. Nishitani, S. Miyazaki, H. Hua, J. Ueda, M. Higuchi, S. Tanabe, Large red-shift of luminescence from BaCN₂:Eu²⁺ red phosphor under high pressure, Appl. Phys. Express. 13 (2020) 9–12. <https://doi.org/10.35848/1882-0786/ab8055>.
- [6] C.E. Tyner, H.G. Drickamer, Studies of luminescence efficiency of Eu²⁺ activated phosphors as a function of temperature and high pressure, J. Chem. Phys. 67 (1977) 4116–4123. <https://doi.org/10.1063/1.435388>.
- [7] T. Tröster, S. Schweizer, M. Secu, J.M. Spaeth, Luminescence of BaBr₂:Eu²⁺ under hydrostatic pressure, J. Lumin. 99 (2002) 343–347. [https://doi.org/10.1016/S0022-2313\(02\)00371-X](https://doi.org/10.1016/S0022-2313(02)00371-X).
- [8] P.J. Wang, H.G. Drickamer, High pressure optical studies of rare earth ions in CaF₂ and other fluorides, J. Chem. Phys. 4444 (1973) 4444–4446. <https://doi.org/10.1063/1.1679005>.
- [9] D.B. Gatch, D.M. Boye, Y.R. Shen, M. Grinberg, Y.M. Yen, R.S. Meltzer, Pressure dependence of the impurity-trapped exciton emission in BaF₂: Eu and Bax Sr_{1-x}F₂: Eu, Phys. Rev. B - Condens. Matter Mater. Phys. 74 (2006) 3–8. <https://doi.org/10.1103/PhysRevB.74.195117>.
- [10] F. Datchi, R. LeToullec, P. Loubeyre, Improved calibration of the SrB₄O₇:Sm²⁺ optical pressure gauge: Advantages at very high pressures and high temperatures, J. Appl. Phys. 81 (1997) 3333–3339. <https://doi.org/10.1063/1.365025>.
- [11] M. Runowski, P. Woźny, V. Lavín, S. Lis, Optical pressure nano-sensor based on lanthanide doped SrB₂O₄:Sm²⁺ luminescence – Novel high-pressure nanomanometer,

- Sensors Actuators, B Chem. 273 (2018) 585–591.
<https://doi.org/10.1016/j.snb.2018.06.089>.
- [12] P. Taylor, B. Lorenz, Y.R. Shen, W.B. Holzapfel, High Pressure Research : An International Characterization of the new luminescence pressure sensor SrFCl : Sm, (n.d.) 37–41.
- [13] H.K. Mao, J. Xu, P.M. Bell, Calibration of the ruby pressure gauge to 800 kbar under quasi-hydrostatic conditions, J. Geophys. Res. 91 (1986) 4673.
<https://doi.org/10.1029/jb091ib05p04673>.
- [14] J.D. Barnett, S. Block, G.J. Piermarini, An optical fluorescence system for quantitative pressure measurement in the diamond-anvil cell, Rev. Sci. Instrum. 44 (1973) 1–9.
<https://doi.org/10.1063/1.1685943>.
- [15] S. Goderski, M. Runowski, P. Woźny, V. Lavín, S. Lis, Lanthanide Upconverted Luminescence for Simultaneous Contactless Optical Thermometry and Manometry-Sensing under Extreme Conditions of Pressure and Temperature, ACS Appl. Mater. Interfaces. 12 (2020) 40475–40485.
<https://doi.org/10.1021/acsami.0c09882>.
- [16] M.A. Antoniak, S.J. Zelewski, R. Oliva, A. Żak, R. Kudrawiec, M. Nyk, Combined Temperature and Pressure Sensing Using Luminescent NaBiF₄:Yb,Er Nanoparticles, ACS Appl. Nano Mater. 3 (2020) 4209–4217. <https://doi.org/10.1021/acsanm.0c00403>.
- [17] M. Runowski, J. Marciniak, T. Grzyb, D. Przybylska, A. Shyichuk, B. Barszcz, A. Katrusiak, S. Lis, Lifetime nanomanometry-high-pressure luminescence of up-converting lanthanide nanocrystals-SrF₂:Yb³⁺,Er³⁺, Nanoscale. 9 (2017) 16030–16037. <https://doi.org/10.1039/c7nr04353h>.
- [18] Y. Wang, T. Seto, K. Ishigaki, Y. Uwatoko, G. Xiao, B. Zou, G. Li, Z. Tang, Z. Li, Y. Wang, Pressure-Driven Eu²⁺-Doped BaLi₂Al₂Si₂N₆: A New Color Tunable Narrow-Band Emission Phosphor for Spectroscopy and Pressure Sensor Applications, Adv. Funct. Mater. 30 (2020) 1–10. <https://doi.org/10.1002/adfm.202001384>.
- [19] N.J. Hess, G.J. Exarhos, Temperature and Pressure Dependence of Laser Induced Fluorescence in Sm: Yag “A New Pressure Calibrant, High Press. Res. 2 (1989) 57–64. <https://doi.org/10.1080/08957958908201032>.
- [20] M. Runowski, A. Shyichuk, A. Tymiński, T. Grzyb, V. Lavín, S. Lis, Multifunctional Optical Sensors for Nanomanometry and Nanothermometry: High-Pressure and High-Temperature Upconversion Luminescence of Lanthanide-Doped Phosphates - LaPO₄/YPO₄:Yb³⁺-Tm³⁺, ACS Appl. Mater. Interfaces. 10 (2018) 17269–17279.
<https://doi.org/10.1021/acsami.8b02853>.
- [21] M. Runowski, P. Woźny, N. Stopikowska, Q. Guo, S. Lis, Optical Pressure Sensor Based on the Emission and Excitation Band Width (fwhm) and Luminescence Shift of Ce³⁺-Doped Fluorapatite - High-Pressure Sensing, ACS Appl. Mater. Interfaces. 11 (2019) 4131–4138. <https://doi.org/10.1021/acsami.8b19500>.